PAGEOPH, Vol. 143, No. 1/2/3 (1994) 0033-4553/94/030359-27$1.50 + 0.20/0

Scaling of Rock Friction Constitutive Parameters: The Effects of Surface Roughness and Cumulative Offset on Friction of Gabbro

CHRIS MARONE[1] and S. J. D. COX[2]

Abstract—We describe experiments in which large (14×40 cm nominal contact area) blocks of gabbro were sheared in a direct shear apparatus at room temperature, 5 MPa normal stress, and slip velocities from 0.1 to 10 μm/s. The apparatus was servocontrolled using a displacement feedback measurement made directly between the gabbro blocks. Two surface roughnesses were studied (rough, produced by sandblasting, and smooth, produced by lapping with #60 grit) and accumulated displacements reached 60 mm. Measurements of surface topography were used to characterize roughness and asperity dimensions. Step changes in loading velocity were used to interrogate friction constitutive properties. Both rough and smooth surfaces showed appreciable displacement hardening. The coefficient of friction μ for rough surfaces was about 0.45 for initial slip and 0.7 after sliding 50 mm. Smooth surfaces exhibited higher μ and a greater tendency for unstable slip. The velocity dependence of friction a-b and the characteristic friction distance D_c show systematic variations with accumulated displacement. For rough surfaces a-b started out positive and became negative after about 50 mm displacement and D_c increased from 1 to 4 μm over the same interval. For smooth surfaces, a-b began negative and decreased slightly with displacement and D_c was about 2 μm, independent of displacement. For displacements <30 mm, rough surfaces exhibit a second state variable with characteristic distance about 20 μm. The decrease in a-b with displacement is associated with disappearance of the second state variable. Our data indicate that D_c is controlled by surface roughness in a complex way, including but not limited to the effect of roughness on contact junction dimensions for bare rock surfaces. The data show that simple descriptions of roughness, such as rms and peak-to-trough, are not sufficient to infer D_c. Our observations are consistent with a model in which D_c scales with gouge thickness.

Key words: Rock friction, constitutive laws, scaling, characteristic friction distance.

Introduction

Laboratory-derived constitutive laws for rock friction have been found to describe a wide range of observations, including the stability of frictional sliding in laboratory experiments (TULLIS and WEEKS, 1986; WONG *et al.*, 1992), the depth of seismic faulting (TSE and RICE, 1986; MARONE and SCHOLZ, 1988), and characteristics of earthquake-like, dynamic rupture (OKUBO, 1989). The success of

[1] Department of Earth, Atmospheric, and Planetary Sciences, Massachusetts Institute of Technology, Cambridge, MA, U.S.A.

[2] CSIRO Division of Exploration and Mining, Nedlands, Western Australia.

modeling this diverse set of phenomena is based in part on the generality of the laws but also on the large uncertainties associated with key constitutive parameters. The uncertainty stems from the great range over which laboratory measurements of these parameters must be scaled when applied to natural faults (SCHOLZ, 1988; MARONE and KILGORE, 1993).

In the context of rate and state-variable friction laws the key scaling parameter is the characteristic friction distance D_c. Along with the slip rate dependence of friction a-b, a dimensionless quantity which is generally taken as scale invariant (TULLIS, 1988; WONG *et al.*, 1992), D_c plays a key role in controlling many important phenomena, including the amount of preseismic slip, the maximum frequency of seismic source radiation, and the size of earthquake nucleation zones (RICE and RUINA, 1983; IDA, 1973; DIETERICH, 1986; OHNAKA and YAMASHITA, 1989).

D_c represents a memory effect of friction for past states of the slipping region and, as such, scales with the slip necessary to effect a change in friction (DIETERICH, 1979). Laboratory measurements of this parameter are generally in the range 10^{-6} to 10^{-5} m (RUINA, 1983; TULLIS and WEEKS, 1986; OHNAKA and KUWAHARA, 1990; MARONE and KILGORE, 1993). In contrast, earthquake modeling studies (IDA, 1973; TSE and RICE, 1986; AKI, 1987; LI, 1987; TULLIS, 1988; RICE, 1993) and field studies (POWER and TULLIS, 1992) yield values of 10^{-3} to 10^{-2} m. Since D_c has been related to the size of surface contact junctions in laboratory experiments (RABINOWICZ, 1951; DIETERICH, 1981) this large discrepancy may arise from differences between the roughness of natural faults and laboratory samples (SCHOLZ, 1988). Alternatively, the discrepancy may arise from differences in the thickness of fault gouge (MARONE and KILGORE, 1993) or other factors.

Mechanics and Scaling of D_c

Two cases may be distinguished when considering the scaling of D_c with surface roughness of laboratory samples. One in which the rock surfaces interact more or less directly and one in which they are separated by a layer of fault gouge which is thick in comparison to the surface roughness. We refer to these as bare surface and gouge cases, respectively.

The interpretation of D_c as the slip distance necessary to completely change contact junctions (DIETERICH, 1981) is consistent with data from bare surface experiments showing larger d_r, a related parameter, for rougher surfaces (OKUBO and DIETERICH, 1984). In this view, rougher surfaces have larger contact junction size and thus require larger slip D_c to erase the memory of past frictional states. However, the database for the roughness effect on D_c for bare surfaces is limited and largely drawn from experiments designed for other purposes. These studies generally did not involve modeling of the effects of elastic interaction between the

fault and loading system, making it difficult to obtain quantitative values for D_c and the other constitutive parameters. Furthermore, detailed measurements of the surface topography and roughness characteristics were not available and thus it is not possible to quantitatively evaluate the link between D_c and surface roughness.

Moreover, in all previous experiments known to us in which detailed measurements were made of friction constitutive parameters, the surfaces studied were relatively smooth (rms roughness of 10–30 μm and peak-to-trough relief of $<80\,\mu$m) and flat at wavelengths above about 1 mm. Since natural faults are extremely rough by comparison (SCHOLZ, 1990) the question arises: will D_c continue to scale with contact junction size at larger scales, or will other factors dominate and limit or change the scaling of D_c with fault roughness?

Distinguishing between such possibilities is an important task since quantitative application of friction laws to natural faults requires tight constraints on the constitutive parameters. Practical limitations on the size of laboratory faults means that the task of providing these constraints is one of scaling measurements on cm- to dm-sized samples to natural faults. This, in turn, requires a detailed physical understanding of the underlying mechanisms operating in both cases.

SCHOLZ (1988) addressed the scaling problem by calculating contact junction size for faults with an arbitrary fractal roughness. Recognizing that the mechanical behavior of surface contacts depends only on the unmated part of the composite roughness spectrum, he calculated the maximum spacing of contacts λ_c and related this to the minimum size of mated junctions. Although he found reasonable agreement between the minimum junction size and estimates of D_c from earthquake modeling, he assumed contact between the surfaces at all wavelengths above λ_c, which is not the case for laboratory experiments on nominally flat surfaces. Moreover, he ignored the role of fault gouge, which has a significant effect on D_c for laboratory faults (MARONE and KILGORE, 1993). Thus, the question remains as to how to scale laboratory measurements of D_c to natural faults.

The purpose of this paper is to address the scaling issue more directly by expanding the sample size and roughness scale studied under laboratory conditions and examining the effect on constitutive parameters of surface roughness and cumulative slip. We also study the relation between surface roughness, asperity characteristics and friction constitutive behavior.

Experimental Technique

Apparatus

The experiments were carried out at the CSIRO Division of Geomechanics in a large direct shear apparatus (Figure 1) described by COX (1990). The apparatus consists of two 100-ton hydraulic rams, which provide shear and normal force on

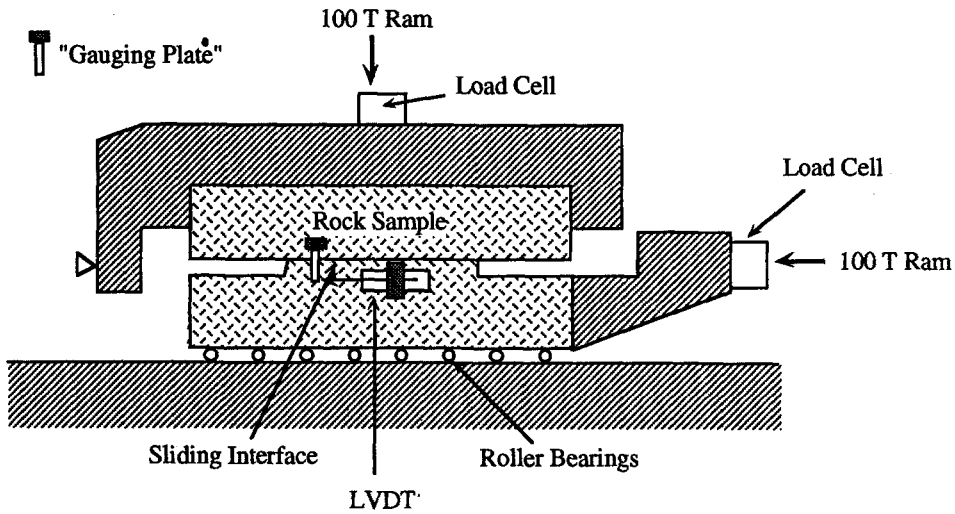

Figure 1
Schematic drawing of the direct shear apparatus. The upper and lower sample blocks are each 58.0 × 24.0 × 15.0 cm. They are held within reinforced steel cradles and sliding is accomplished by rolling the lower cradle beneath the stationary upper cradle. The lower cradle moves on specially designed, low-friction roller bearings. To measure shear displacement between the rock samples, LVDT's and gauging plates were attached directly to the blocks close to the sliding interface. The measurement was made on both sides of the sample to check for misalignment.

rock samples held within reinforced steel cradles. Frictional sliding is accomplished by rolling the lower cradle on low-friction roller bearings while the upper rock sample is held stationary (Figure 1). Both the vertical and horizontal rams are servocontrolled. Our experiments were carried out at constant normal stress of 5 MPa and specified shear displacement rates from 0.1 to 10 μm/s. The control transducer for shear displacement was attached directly to the rock, close to the sliding interface (Figure 1), effectively eliminating distortion of the apparatus from the quasi-static loading stiffness. Measurements of shear stress and displacement during loading indicate that the machine stiffness is 0.170 MPa/μm.

We assessed the inherent velocity dependence of roller bearing friction by measuring the force necessary to roll samples at different velocities (see Figure 1). For these tests, the upper cradle was removed and the top rock sample rested on the lower sample to increase normal load on the bearings. A 10× change in rolling velocity required a maximum increase in horizontal force equivalent to a shear stress on the sliding surface of 0.0003 MPa, or a change in coefficient of friction of 6×10^{-5} for a normal stress of 5 MPa. This is a factor of 10 or more smaller than the measurements of friction velocity dependence reported below.

A high-speed datalogger was used to record horizontal and vertical load, displacement of the vertical ram, and slip between the rock samples at evenly

spaced slip intervals. Data were generally recorded every 0.5 microns of shear displacement.

Rock Samples

We used a medium-grained, alkali-rich gabbro (Imperial Gabbro from South Australia), consisting of plagioclase, clinopyroxene, Fe-Ti-oxide, biotite, and interstitial, microperthitic K-feldspar. The average grain diameter of Imperial Gabbro is 2 mm and most plagioclase and clinopyroxene grains are between 1 and 5 mm in longest dimension. Biotite is mainly primary and apatite is a common accessory phase. Plagioclase occurs as euhedral crystals with lamellar twinning and weak zoning. Clinopyroxene is subhedral and has exsolution lamellae of orthopyroxene. Serpentinization, clays or other evidence of alteration were not found.

The sample dimensions were $58.0 \times 24.0 \times 15.0$ cm. Each sample surface was ground square and parallel. The upper surface of the bottom sample was cut so that the frictional contact area (nominally 14×40 cm) remained constant during slip (Figure 1) Because of the time necessary to prepare the samples and surfaces, the data presented in this paper are for only two samples, one rough and one smooth. A third sample was prepared with smooth surfaces and the results were similar to those described below, although detailed data modeling and roughness characterization were not carried out.

Surface Roughness

Surfaces were ground flat and parallel with a surface grinder and roughened by lapping with #60 silicon-carbide grit (smooth) or sandblasting (rough). Sandblasting was done with garnet sand using a large, commercial sandblaster and a working distance of about 1 m. This provided a spray diameter slightly larger than our surface width (14 cm). Our roughness was produced in three sweeps of the surface each lasting about 5 seconds.

The topography of each surface was measured along linear profiles parallel and perpendicular to the sliding direction with an LVDT which traversed the surface in continuous contact, as with a stylus profilometer. Surface height was sampled every 25 μm with a vertical resolution of 0.1 μm (Figure 2). The profiles show that the samples remained flat overall after surface preparation and that the sandblasted surfaces had significantly greater roughness than the surfaces prepared with #60-grit.

From these profile data we calculated asperity characteristics using the methods of YOSHIOKA and SCHOLZ (1989) and YAMADA *et al.* (1978). Their method yields idealized asperity geometries (see inset to Figure 3c) from profile topographic data, accounting for the effects of traversing asperity shoulders more frequently than true summits.

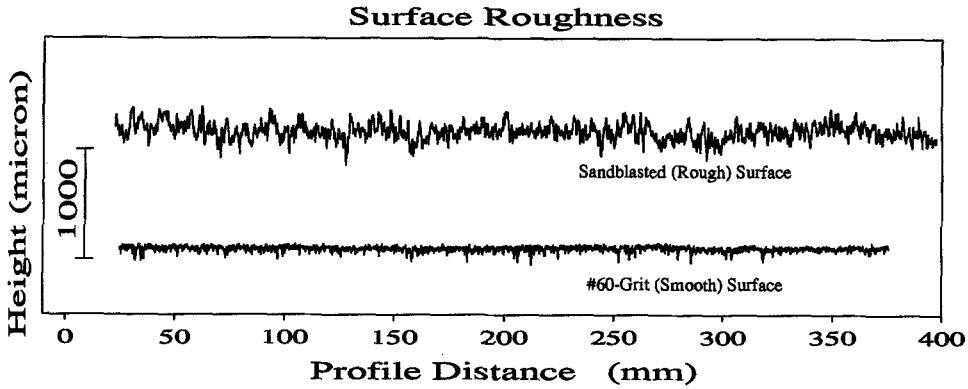

Figure 2

Topography of the rough and smooth surfaces, as measured along linear profiles parallel to the sample's long axis. Note greater amplitude and longer wavelength roughness of the sandblasted surface. The sample interval is 25.0 μm and height resolution is about 0.1 μm. Power spectra for these profiles are shown in Figure 4b and asperity characteristics for each surface are given in Figures 3 and 4a. Average roughness characteristics are given in Table 1.

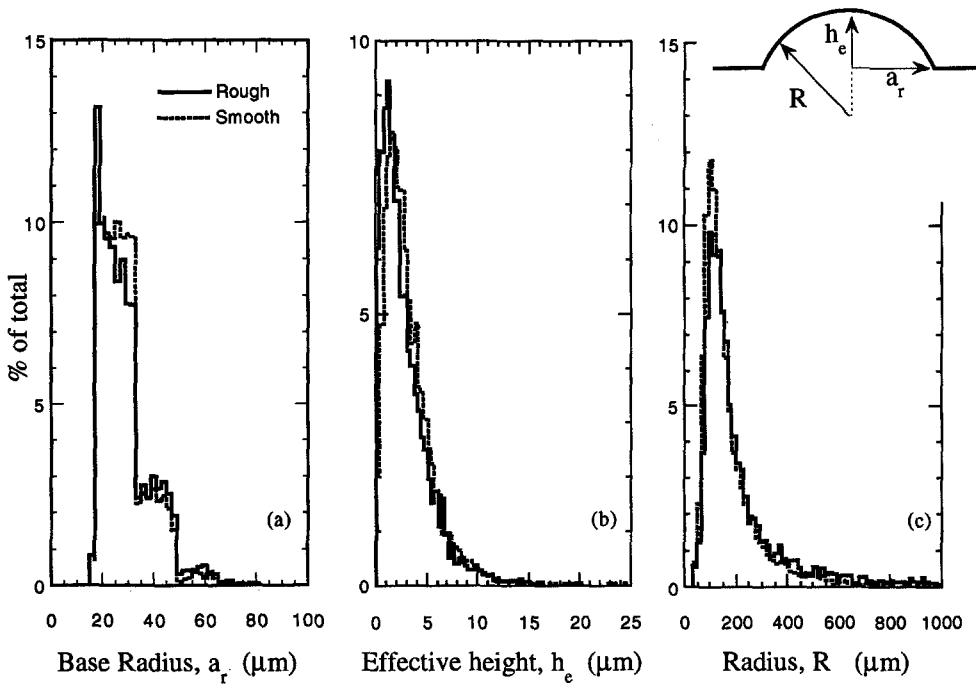

Figure 3

Asperity characteristics for the rough and smooth surfaces as computed from profiles such as shown in Figure 2. Inset to (c) shows idealized asperity geometry. R is asperity radius, h_e is its height above the surrounding surface and a_r is the base radius. The data represent composite characteristics of summits observed along several profiles of each surface. The ordinate is the percentage of the total number of asperities (3000 to 5000) observed on each surface.

Rough and smooth surfaces have similar distributions of asperity radius a_r, effective height h_e, and base radius R (Figure 3). Since contact characteristics are likely to be dominated by the most abundant asperities we focus primarily on the mode of the distributions. Smooth surfaces have slightly smaller radius and slightly larger effective height (Table 1). These values are consistent with the observation of smaller mean base radius for smooth surfaces, but not with larger mode, which is poorly determined for the relatively flat-topped distribution of smooth surfaces (Figure 3). The distribution of asperity radii for rough surfaces has a rather long tail extending to values $>1000\,\mu$m, reflecting larger, broader asperities in the rougher surfaces (Figure 2).

Differences in the asperity characteristics of the two surfaces are more apparent from the distribution of asperity heights relative to the highest asperities (Figure 4a). Summit depth is the distance of an asperity summit below the highest asperity and, as such, represents the depth of a summit below the contact the surface would make with an idealized flat surface. Smooth surfaces show a much narrower summit depth distribution than rough surfaces, reflecting an asperity population which would, on average, be closer to a contacting surface.

The rough surfaces have rms and peak-to-trough roughnesses about four times greater than smooth surfaces (Table 1). We also report the parameter λ_c, which is the maximum asperity radius, and thus the maximum contact spacing (SCHOLZ, 1988). λ_c corresponds to about the corner frequency of the roughness power spectra (Figure 4b). KUWAHARA *et al.* (1988) reported λ_c values from power spectra of #60-grit surfaces and found values similar to ours. Our rough surfaces have significantly higher spectral power and contain longer wavelength roughness than the smooth surfaces.

Constitutive Law

We interrogated friction constitutive behavior using the method of step changes in load point velocity (e.g., DIETERICH, 1979, 1981; TULLIS and WEEKS, 1986). We

Table 1

Surface topography data

	Surface roughness			Asperity size					
	rms μm	Peak-to--trough μm	λ_c mm	Radius μm mode	Radius μm mean	Effective height μm mode	Effective height μm mean	Base radius μm mode	Base radius μm mean
#60-grit (smooth)	21.6	186.8	3.28	95	202	1.6	3.1	30	27.7
Sandblasted (rough)	83.3	509.8	12.66	108	337	1.1	2.8	25	28.0

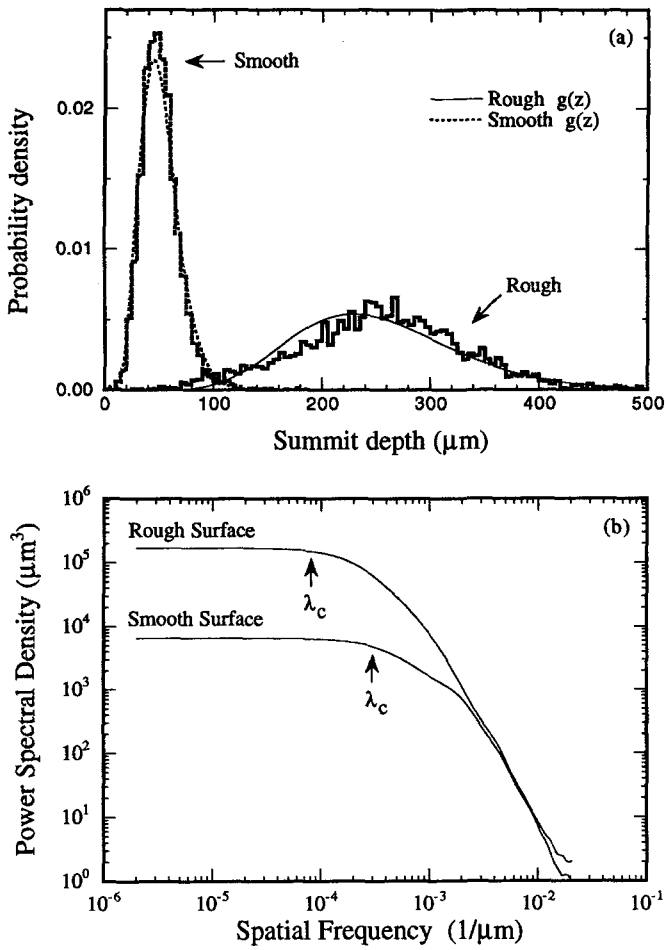

Figure 4

Surface topography data for the rough and smooth surfaces. (a) Depth of asperity summits below the highest asperities. The data show that smooth surfaces have few asperities more than 80–90 μm below the highest peaks. Most asperities on the rough surfaces are 200–300 μm below the highest peaks. Thin lines show the fit to data (thick lines) of a gamma distribution $g(z)$. (b) Power spectra of the roughness profiles shown in Figure 2, calculated using an all poles (maximum entropy) method (PRESS *et al.*, 1988). λ_c is the maximum asperity radius and thus represents the largest contact spacing. The sandblasted surfaces have higher spectral power, which is consistent with greater rms and peak-to-trough roughness than #60-grit surfaces (see Table 1).

modeled data using the rate and state variable constitutive law of DIETERICH (1979) and RUINA (1983):

$$\mu = \mu_0 + a \ln(V/V_*) + b_1\psi_1 + b_2\psi_2, \tag{1}$$

$$\frac{d\psi_i}{dt} = -\frac{V}{D_{ci}}[\psi_i + \ln(V/V_*)], \quad i = (1, 2) \tag{2}$$

where μ_0 is the coefficient of friction at a reference velocity V_0, a and b are, respectively, the magnitude of the instantaneous and displacement-dependent changes in friction for a change in velocity from V_0 to $V = eV_0$, and D_c is the characteristic distance over which friction and the state variable ψ evolve following the velocity change. In some cases, two state variables are required to fit experimental data (BLANPIED and TULLIS, 1986; COX, 1990) and then b, D_c, and ψ take on the subscript i as in equations (1) and (2). The steady-state velocity dependence of friction is given by $a - \Sigma b_i = \Delta\mu/\ln(V/V_*)$.

To model laboratory data, equations (1) and (2) are coupled with a law describing elastic interactions between the frictional surface and its surroundings:

$$d\tau/dt = K(V_0 - V), \tag{3}$$

where τ is shear stress and K is stiffness. The system of equations (1–3) are solved numerically to yield friction vs. displacement curves for comparison with data. As these relations and their application and limitations have been discussed extensively in the literature (see TULLIS, 1988 and SCHOLZ, 1990 for recent reviews) the reader is referred there for additional information.

Data Inversion

We obtained values for the constitutive parameters using an iterative inverse technique to fit relations (1–3) to data. Our method uses a steepest-descent, simplex algorithm, which iteratively adjusts model parameters to minimize the chi-squared error between a simulation and data (e.g., PRESS *et al.*, 1988). The method is therefore less efficient than those using higher-order derivatives of the error with respect to the constitutive parameters (REINEN and WEEKS, 1993), however a typical velocity step contains < 500 data points and thus this inefficiency did not represent a major problem. We calculated the error between a simulation and data at the recorded shear displacements by adjusting the step size of the numerical calculation after it had exceeded a given displacement and restarting the calculation from the previous displacement.

The inversion for each data set was started with a two state variable model, although in nearly all cases a degenerate one state variable model (i.e., $D_{c1} = D_{c2}$ or $b_2 = 0$) was the eventual best fit. Cases in which the inversion converged with $D_{c1} = D_{c2}$ indicate that one state variable is sufficient to describe the data and thus the sum of b_1 and b_2 was taken as b_1.

For about half of the data linear trends were present in the friction load point displacement curves, representing displacement hardening or weakening. Since the rate and state variable friction law is not intended to model such trends one must choose between adding a linear term to the law or removing the trend from the data and modifying the apparent stiffness used for the numerical simulations. The latter approach is more straightforward, however, it can lead to problems in cases where

the system is close to the critical stiffness. We used this approach because of the small stiffness correction required for our data. Our machine stiffness (shear stress/shear displacement) is 0.170 MPa/μm and thus a displacement hardening trend of 1×10^{-5} μm^{-1} results in an apparent stiffness of 0.16995 MPa/μm. We removed linear trends in the friction-displacement data if the slope exceeded $|5 \times 10^{-6}$ $\mu m^{-1}|$ which was the case in about 50% of our data.

We inverted for the parameters a, b_i and D_{ci} using the measured value of a-b as a constraint. A number of trials were made in which we also inverted for a-b instead of fixing it. These produced values of a-b which were essentially identical to the measured values and thus it was decided to fix a-b in the inversions. To improve the fit to the instantaneous friction response relative to later data we weighted initial points around the direct effect of the velocity step.

Reproducibility in determining model parameters with our inverse technique was estimated by: 1) starting the inversion with different initial values; for example: a (0.005–0.03), b_1 (0.005–0.03), D_{c1} (5–50), D_{c2} (50–200), and 2) comparing the chi-square error and overall fit (by eye) of the model to data. Inversions typically converged to parameter values within 10%. The error bars shown in the figures below are maximum estimates of modeling error. This error is generally small compared with scatter and systematic trends in the experimental data.

Data

For both the rough and smooth samples, cumulative slip of 50–60 mm was imposed in a series of sliding episodes of length 2–5 mm (Figure 5). The shear and normal loads were removed between episodes. After reapplication of normal load, shearing began with an increase in shear load followed by an inflection in the friction-displacement curve indicating the onset of sliding. Rough surfaces showed a gradual onset of sliding for small accumulated displacements. With increasing displacement, friction-displacement curves generally showed a sharp onset of sliding and in some cases a distinct peak stress (Figures 5 and 6).

Between a few slip episodes the top sample block was lifted and the lower block retracted, so that further slip occurred within a previously worn region of the upper surface (Figure 1). The positions at which retractions were done are indicated by the arrows along the abscissa on Figures 5, 10, and 11. They had the effect of making the onset of sliding more gradual in the next slip episode but otherwise did not have a significant effect on the frictional behavior (Figure 5).

On a scale of cm's of sliding, rough surfaces exhibited significant slip hardening, with friction increasing from about 0.45 upon initial slip to 0.7 after cumulative slip of 53 mm (Figures 5 and 6). Within a given sliding episode the slip hardening was small (Figure 6) and comparable to that observed by others (TULLIS and WEEKS, 1986).

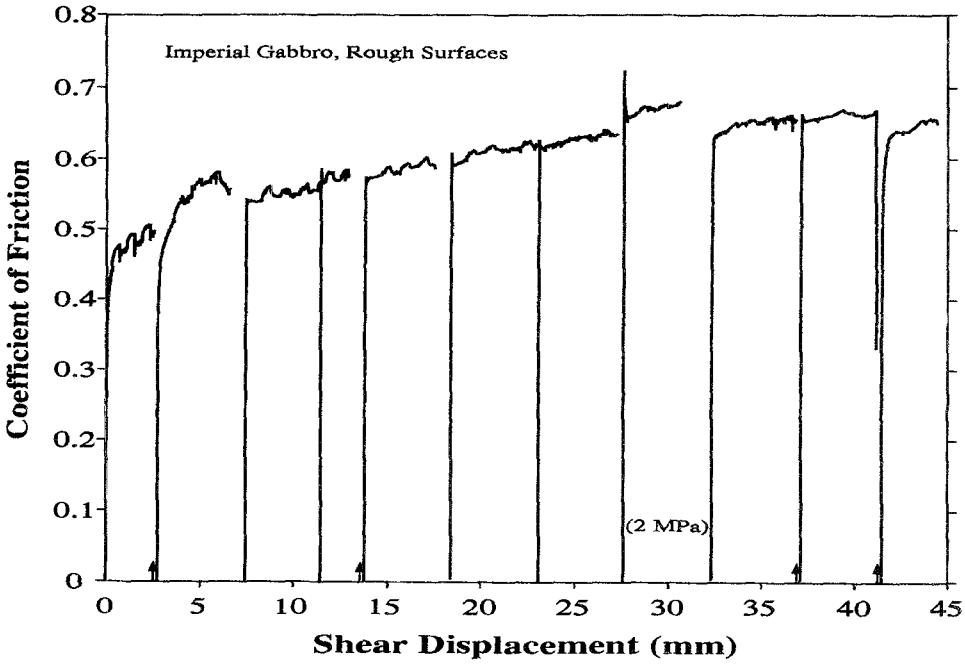

Figure 5
Coefficient of friction (shear stress/normal stress) is plotted vs. shear displacement for a series of slip episodes using rough surfaces. Shear and normal load were removed between each slip episode. Minor variations in friction during sliding represent the effects of changes in slip rate. The data show significant slip hardening during the first 25–30 mm of slip. Data from the first slip episode are also shown in Figure 6. The slip episode beginning at a displacement of 27 mm was done at 2 MPa normal stress, as indicated by the annotation. Arrows along the abscissa indicate points at which the top sample block was lifted and the lower block retracted, so that further slip occurred within a previously worn region of the upper surface.

The slip-rate dependence of friction evolved with accumulated displacement (Figure 6). For small displacements, the steady-state friction level (e.g., the level after the transient change in friction, which we describe below) increased with increasing slip rate, exhibiting velocity strengthening. These transients and the steady-state change with slip rate can also be seen at the scale of Figure 5. With increasing displacement, the magnitude of the transient effect and of the velocity strengthening decreased, and steady-state friction became approximately independent of velocity (Figures 5 and 6).

Smooth surfaces showed much less slip hardening than rough surfaces. Friction of the smooth surfaces was about 0.6 upon initial slip and increased to about 0.72 and 0.76 after net slip of 12 mm and 51 mm, respectively (Figure 7). Smooth surfaces showed velocity-weakening friction for all displacements and a greater tendency for unstable sliding with increasing net slip.

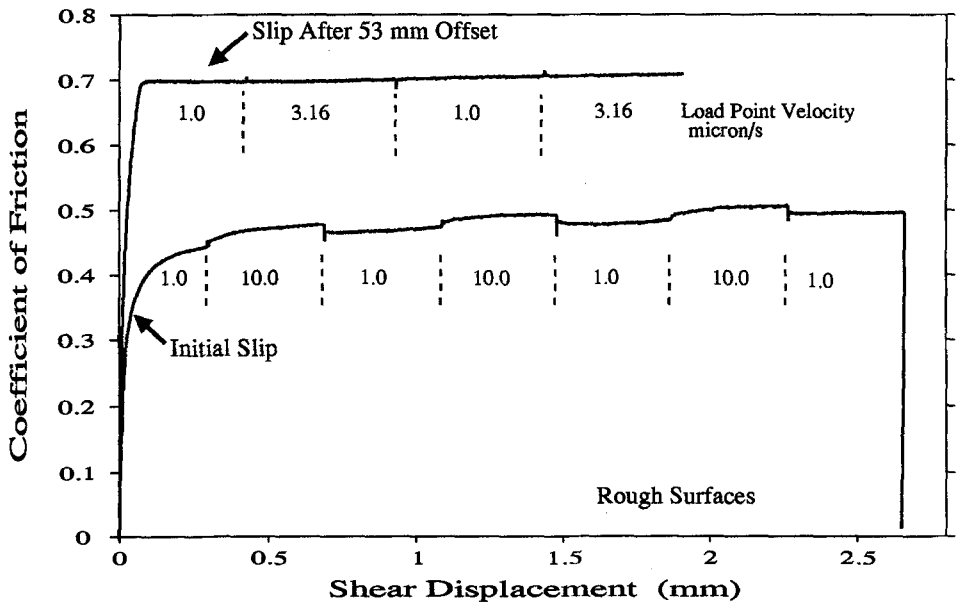

Figure 6
Friction data for rough surfaces. The first slip episode of Figure 5 is shown with data from slip that began after a cumulative offset of 53 mm. The absolute friction level is significantly higher for larger net slip. Numbers below each curve show load point velocity. For low net slip, steady-state friction increases with slip rate (velocity strengthening). For larger net slip, the steady-state friction level is approximately independent of velocity or decreases slightly with velocity (velocity weakening).

Constitutive Modeling

The friction response to a step change in load point velocity was similar to that observed by others for a variety of rock types and fault gouges sheared under a range of temperatures and pressures (DIETERICH, 1981; TULLIS and WEEKS, 1986; LOCKNER *et al.*, 1986; MARONE *et al.*, 1990; COX, 1990; REINEN *et al.*, 1991; BLANPIED *et al.*, 1991; CHESTER, 1993; REINEN *et al.*, 1994; WANG and SCHOLZ, 1994).

We imposed changes in load point velocity after an approximately steady-state friction level had been reached. Upon a change in load point velocity the initial change in friction (the so-called direct effect) was of the same sign as the velocity change (Figures 6–8). This was followed by an evolution effect of opposite sign (Figure 8). For rough surfaces and low net displacements, the direct effect was of larger magnitude than the evolution effect, resulting in velocity strengthening.

Rough Surfaces

For slip between rough surfaces we modeled 61 velocity steps using the inversion routine described above. Three inversions were done for each data set, using different starting values for the parameters a, b_i, and D_{ci}.

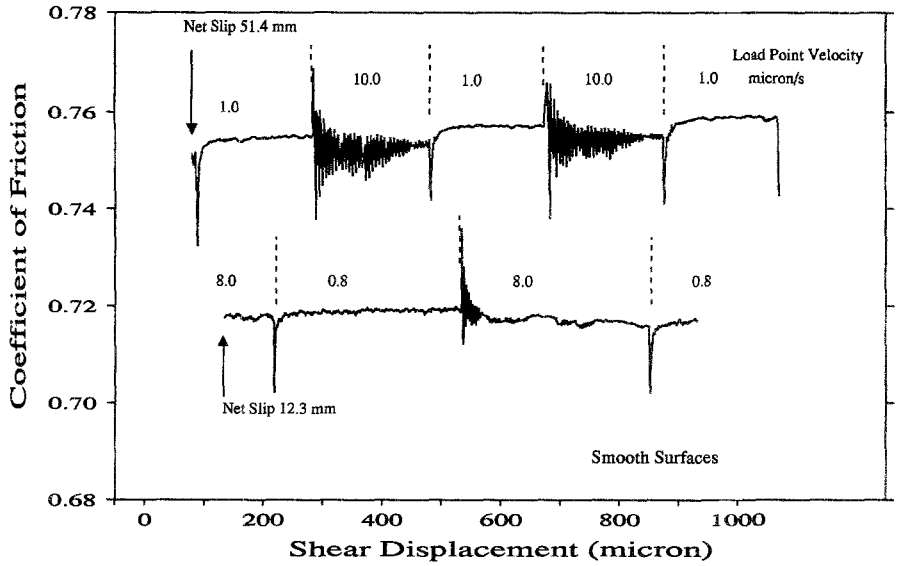

Figure 7
Data for smooth surfaces showing the increase in friction with net slip. The steady-state friction level decreased with velocity (velocity weakening) for all displacements. Smooth surfaces exhibited a greater tendency for unstable sliding (as in the 10.0 μm/s intervals in the upper trace) with increasing net slip.

For relatively low net displacements rough surfaces exhibited two state variable evolution, consisting of a sharp initial change following the direct effect (positive b_1) and a more gradual change of opposite sign (negative b_2). Thus, for a decrease in load point velocity (Figure 8), friction exhibited a steep drop (direct effect) followed by a sharp increase (b_1 effect) and a longer period decay (b_2 effect). With increased net displacement the sharpness of the initial evolution effect diminished and the magnitude of the b_2 effect and second state variable diminished (Figures 8 and 9).

In a few cases, although the best fit model from the inversion had $D_{c1} = D_{c2}$, a second state-variable evolution effect can be seen in the data (Figure 8). In these cases, noise in the data near the velocity step or noise which occurred soon after (and limited the data that could be used in the inversion) generally contributed to the uncertainty between a one- and a two-state variable model. The issue of whether a second state variable is required, however, did not degrade our estimate of D_{c1}, which the data shown has to be about 1 μm (Figure 8).

For rough surfaces and net displacements greater than 30–40 mm, the best fit simulation was a degenerate one state variable model (Figures 9 and 10). With increasing displacement, rough surfaces exhibited reduced velocity strengthening (a-b) and a transition to velocity weakening (Figures 9 and 11). Over the same interval, D_c increased from about 1 μm to 3–4 μm (Figure 11). The decrease in a-b

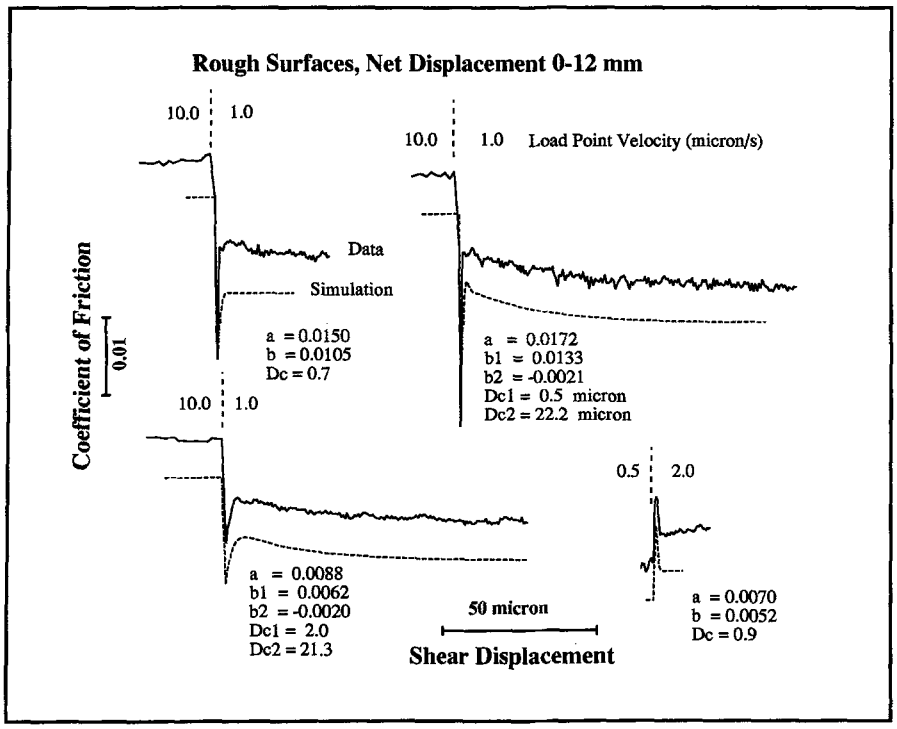

Figure 8

Friction data and numerical simulations for rough surfaces and net displacement < 12 mm. In each case data represent the friction response to a step change in load point velocity (as indicated by the velocities above each data set). Simulations were obtained using an iterative least squares inversion of equations (1–3) to the data. Note the sharp initial evolution effect followed by gradual evolution of opposite sign. Data are arranged with increasing net displacement from left to right and top to bottom.

was the result of an increase in the net evolution effect, with the Σb_i increasing from about 0.004 to 0.01 over the displacement interval 0–60 mm (Figures 9 and 10).

Smooth Surfaces

We modeled 28 velocity steps for slip between smooth surfaces. These exhibited one state variable behavior for all displacements, with the exception of a few cases in which a very small magnitude second evolution effect was present (Figures 12 and 13). These were small enough ($b_2 < 0.001$) that we decided for consistency to use the one state variable fits.

Like the rough surfaces, smooth surfaces showed a sharp initial evolution effect following the direct effect (Figure 12). The parameter a was about the same for rough and smooth surfaces within the scatter in the data. Smooth surfaces did not exhibit the extremely small D_c values sometimes observed for rough surfaces,

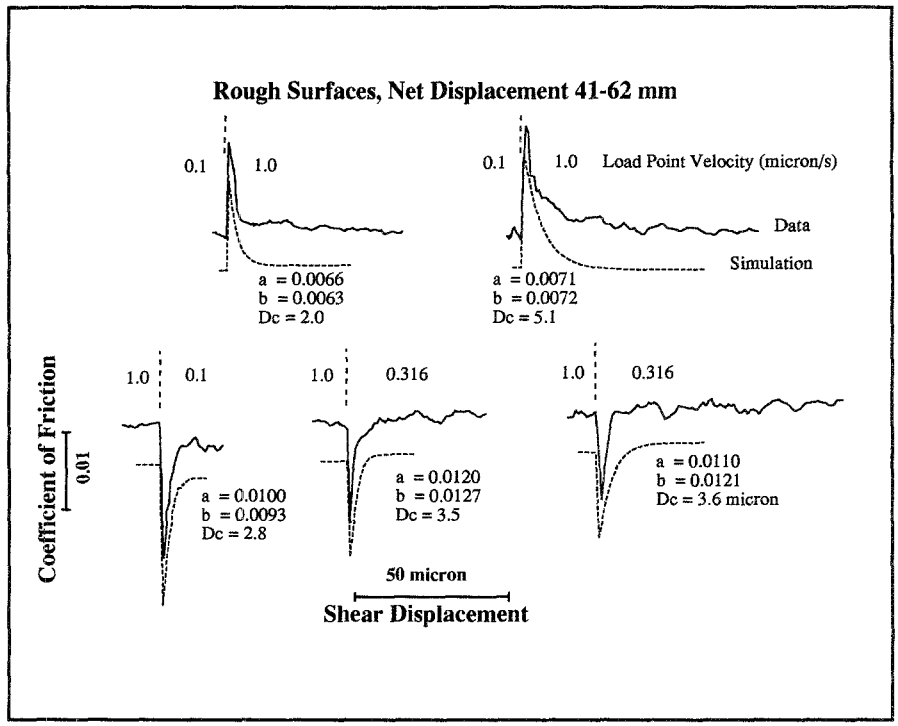

Figure 9

Friction data and numerical simulations for step changes in load point velocity with rough surfaces and large net displacement. Data are arranged with increasing net displacement from left to right and top to bottom. With increasing displacement the magnitude of the friction evolution effect increases (note increase in b) and the friction velocity dependence becomes negative (see Figures 9 and 10).

however the values are comparable within the scatter in the data. We did not attempt to model unstable behavior such as indicated by the oscillations seen in Figure 7, but instability would imply neutral or slightly negative a-b as indicated by the mean value of the decaying oscillations.

For smooth surfaces the magnitude of a and b was approximately independent of displacement within the scatter in the measurements (Figure 14). Measurements of a-b over the interval 10–60 mm showed a small change, from velocity neutral or slightly velocity weakening to velocity weakening (Figure 15). The parameter D_c for smooth surfaces was about 2 μm, independent of displacement within the scatter in the data.

Discussion

Comparison of the constitutive parameters for rough and smooth surfaces shows several important results. First, for small displacements D_{c1} is independent of

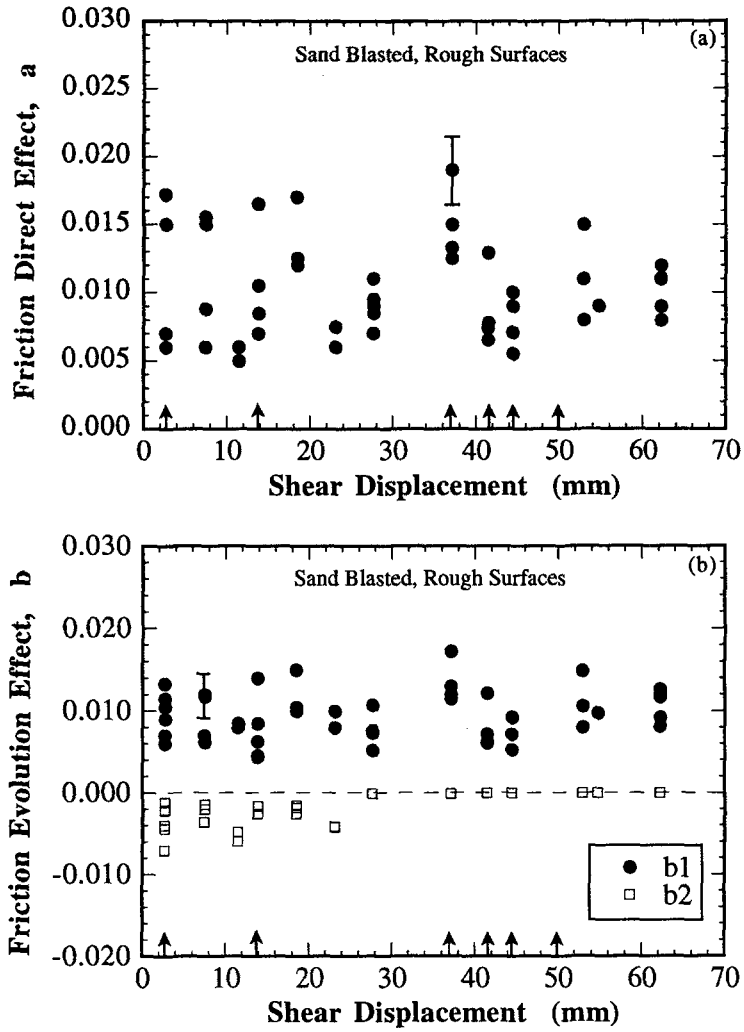

Figure 10

Friction constitutive parameters for rough surfaces as determined by modeling (see Figures 8 and 9). The parameter b_2 represents a gradual friction evolution of the same sign as the velocity change and the sum of b_1 and b_2 is the net evolution effect. Note that b_2 diminishes with displacement and that the data indicate one state variable behavior ($b_2 = 0$) for displacements > 30 mm. Data are plotted at shear displacement corresponding to the beginning of the slip episode (see Figure 5). Error bars in this and the following figures represent aggregate uncertainty of measurement resolution and constitutive modeling. Arrows along the abscissa indicate points at which the top sample block was lifted and the lower block retracted, so that further slip occurred within a previously worn region of the upper surface.

surface roughness. Within the uncertainty in the data, surfaces with a four-fold difference in rms and peak-to-trough roughness have about the same D_{c1} for net displacements less than about 40 mm. Since the surfaces are likely to be significantly modified by wear and gouge accumulation with increasing slip, the effects of contact

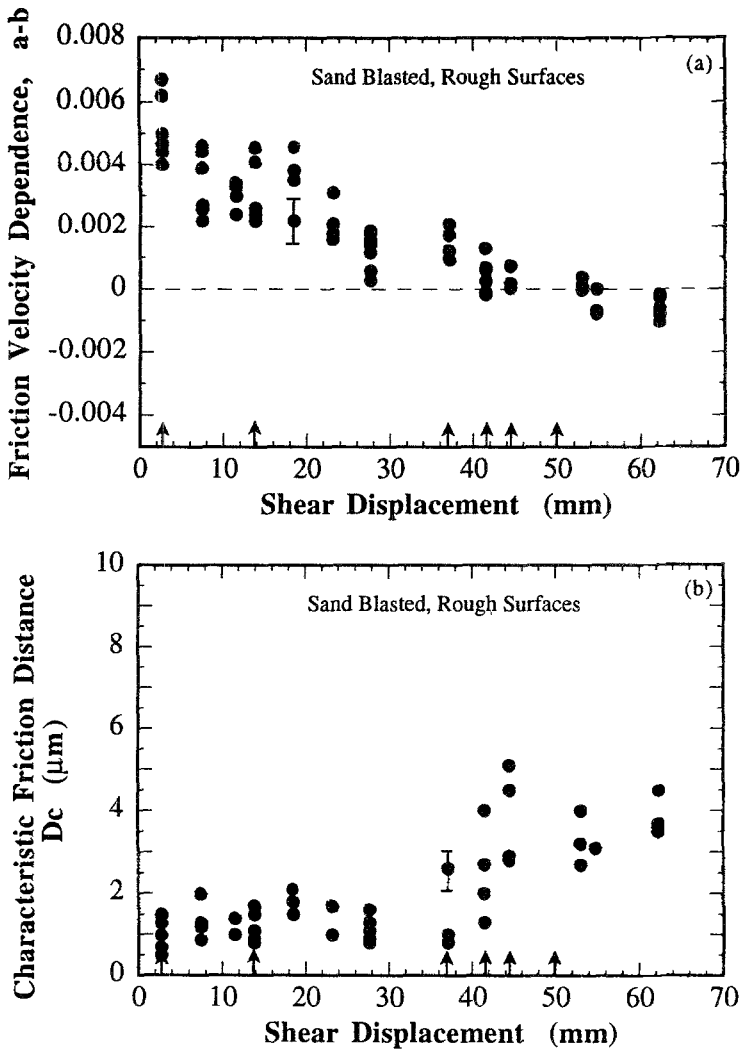

Figure 11

Friction constitutive parameters for rough surfaces as determined by modeling (see Figures 8 and 9). The parameter $a-b$ represents the velocity dependence of friction and decreases with accumulated shear displacement. D_c represents the characteristic distance over which friction evolves following a change in velocity (e.g., see Figures 8 and 9). Data are plotted at the shear displacement corresponding to the beginning of the slip episode (see Figure 5). Arrows along the abscissa indicate points at which the top sample block was lifted and the lower block retracted, so that further slip occurred within a previously worn region of the upper surface.

junction size on friction are best indicated by the data for small displacements. Thus, to the extent that contact size scales with roughness, our data do not support a scaling between D_{c1} and contact size (as discussed below, an alternative interpretation is that D_{c1} is a property of the gouge and D_{c2} scales with roughness).

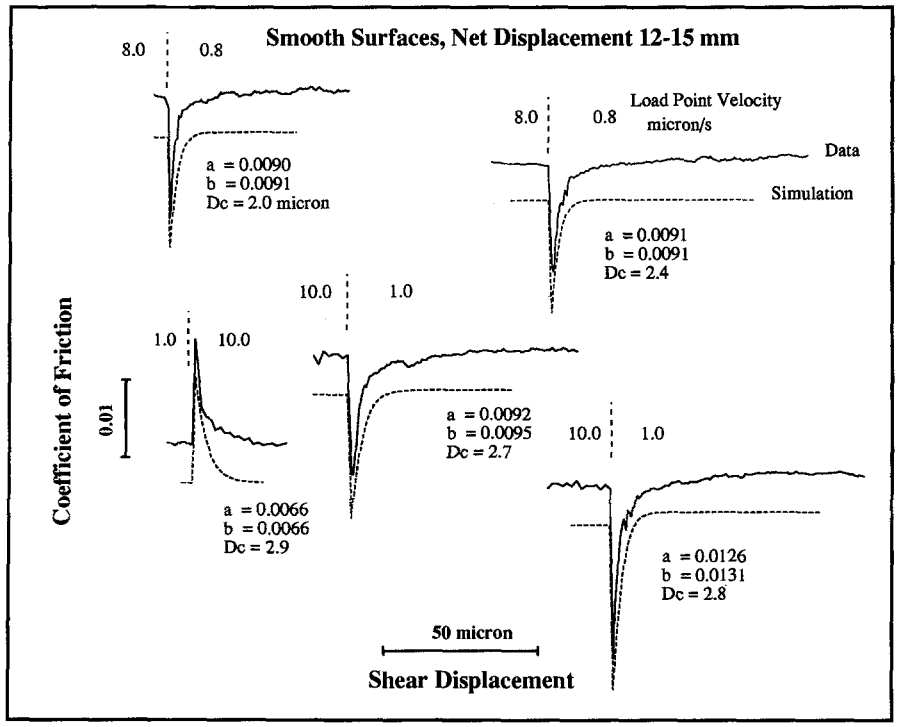

Figure 12

Friction data and numerical simulations for smooth surfaces and low net displacement. In each case data represent the friction response to a step change in load point velocity (as indicated by the values above each data set). Simulations were obtained using an iterative least squares inversion of equations (1–3) to the data. Data are arranged with increasing net displacement from left to right and top to bottom. The data show velocity weakening for all displacements.

If the comparison is somewhat relaxed, and we consider an aggregate D_c (including both D_{c1} and D_{c2}), rough surfaces show larger D_c (20 μm) than smooth surfaces (2 μm) for small displacements. This may explain why OKUBO and DIETERICH (1984) reported larger values of d_r for rougher surfaces, since d_r is the total slip required for friction to reach a new steady-state level following a change in velocity and thus would include both D_{c1} and D_{c2}. Note that D_c and d_r are not strictly equivalent, since d_r is not obtained by modeling and does not include the effect of finite stiffness of the experimental apparatus, so the values should not be compared directly.

The lack of a clear roughness effect on D_{c1} is perhaps not surprising in view of the similarity in asperity characteristics between the two surfaces (Table 1). The topographic profiles show that the sandblasted and 60-grit surfaces have essentially the same idealized asperity size (Figure 3), although the summit depth distributions clearly differ (Figure 4a). In the context of models in which D_c is

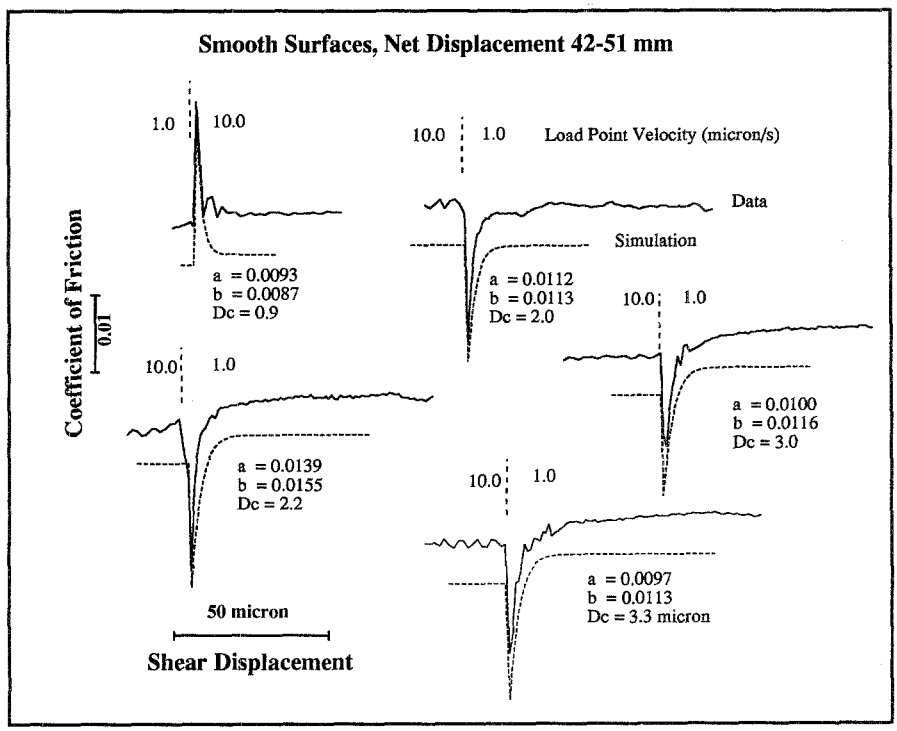

Figure 13
Friction data and numerical simulations for step changes in load point velocity with smooth surfaces and large net displacement. Data are arranged with increasing net displacement from left to right and top to bottom. The magnitude of a-b increases slightly with displacement.

controlled by contact junction size, our results imply that mode and mean summit depth, rms roughness, and peak-to-trough roughness are not good indicators of contact junction size. This is consistent with results from contact theory showing that small asperities, present on larger asperities, play an important role in controlling contact dimensions and friction (ARCHARD, 1957; YOSHIOKA and SCHOLZ, 1989).

Despite the lack of a roughness effect on D_{c1} for small displacement, the friction results as a whole indicate significant differences between the rough and smooth surfaces. Rough surfaces show lower initial friction, greater slip hardening, and a different displacement dependence of a-b than smooth surfaces. Rough surfaces also exhibit velocity strengthening behavior during initial slip, in contrast to smooth surfaces. These results are consistent with previous work showing roughness effects on rupture acceleration (KUWAHARA *et al.*, 1988), stress drop, and rupture velocity (OKUBO and DIETERICH, 1984).

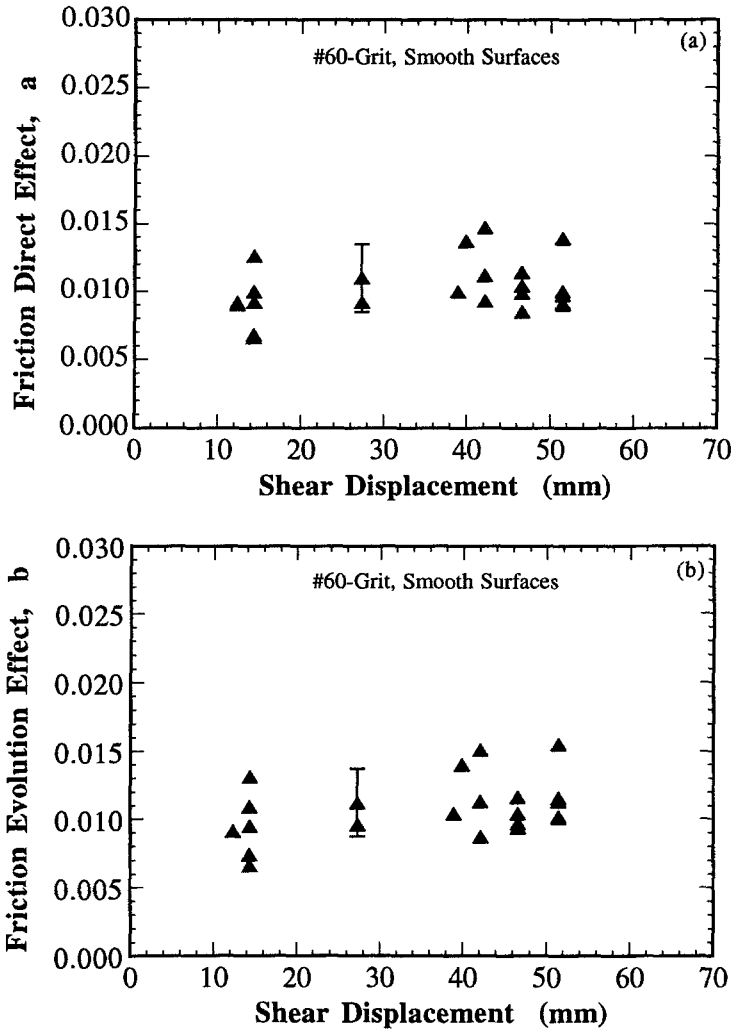

Figure 14

Friction constitutive parameters for smooth surfaces as determined by modeling (see Figures 12 and 13). The friction evolution effect increases slightly with displacement, resulting in a slight decrease in a-b (see Figure 15). a and b (compare b_1) are approximately independent of roughness, whereas for low displacements the net evolution effect is lower than that for rough surfaces (compare Figure 10). Data are plotted at the shear displacement corresponding to the beginning of the slip episode.

Assumption of Quasi-static Slip

One possible explanation of our results is that small D_c values are the result of inertial overshoot upon a velocity decrease (e.g., PISARENKO and MORA, 1994). That is, an important assumption inherent in equation (3) is that-the mass of the sliding elements may be ignored and that slip is quasi-static. For many experimental

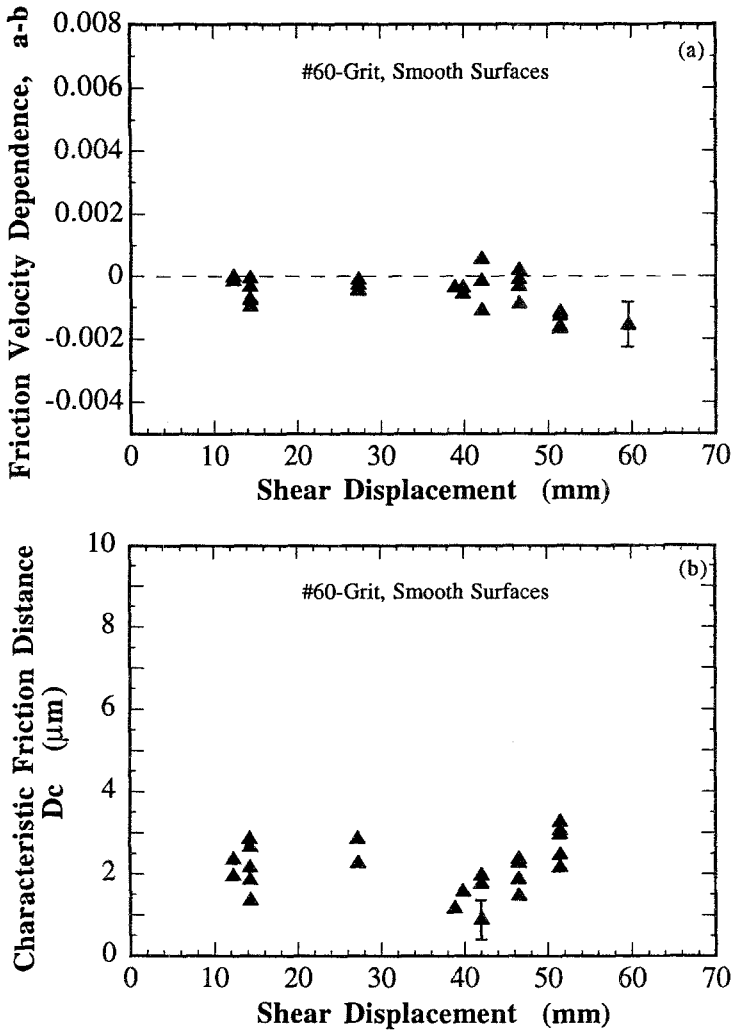

Figure 15

Friction constitutive parameters for smooth surfaces as determined by modeling (see Figures 12 and 13). a-b decreases slightly with displacement. For displacements <40 mm, a-b is lower than that for rough surfaces, whereas for larger displacements a-b is approximately independent of roughness. D_c is approximately independent of displacement. Data are plotted at the shear displacement corresponding to the beginning of the slip episode.

configurations this is justified by the use of small samples of negligible mass. However, in the present case the sliding elements (lower cradle and sample) have mass of about 450 kg. The following analysis is therefore useful for understanding possible limitations of our quasi-static analysis.

RICE and TSE (1986) showed that a quasi-static analysis is valid when $T/2\pi \ll D_c/V$, where T is the system's natural period of vibration. This result can be

understood by noting that the constitutive law (1–2) requires a finite slip (on order D_c) to effect a change in friction. Thus, if the slip during half of the natural vibrational period $VT/2$ is large compared with D_c a significant change in friction can be expected, whereas the opposite implies negligible change in friction and thus negligible acceleration.

For our system, $K = 1.11 \times 10^{10}$ N/m (which is 0.170 MPa/μm when written as an equivalent shear stress per displacement on the sliding surface) and the sliding mass $m = 450$ kg. Assuming the system vibrates with no damping, $T = 2\pi(m/K)^{1/2}$, which for our system yields $T/2\pi = 2.02 \times 10^{-4}$ s. Damping due to frictional resistance between the rock surfaces would increase this value. Thus, for our range of velocities, if D_c is in the range 1–10 μm D_c/V is 10^{-1} to 10^{2} s, which is well within the quasi-static range.

Comparison with Previous Work

Our observations of positive a-b for rough surfaces and decreasing a-b with slip are consistent with previous work. DIETERICH (1981) reported similar results for shear of simulated fault gouge and attributed it to comminution and a general "running in" phase associated with the achievement of a steady frictional strength. Subsequent work (BIEGEL *et al.*, 1989; BEELER *et al.*, 1993; MARONE and KILGORE, 1993) supports this view in a general way, showing decreasing a-b with displacement. However, MARONE (1993) showed that comminution alone cannot explain the evolution of a-b and argued that shear localization plays a more fundamental role.

Moreover, it has to be noted that our surfaces were initially bare, whereas the others noted above involved a layer of simulated fault gouge. As noted by TULLIS and WEEKS (1986), the evolution with slip of a-b may differ for the two cases. They found negative and increasing a-b with displacement for initially-bare, granite surfaces. They used #80-grit surfaces (somewhat smoother than our smooth surfaces) and reported steady-state a-b values of -0.001 to -0.002 after 50–70 mm of displacement. This value is similar to DIETERICH'S (1981) a-b value for shear of gouge and to our values for smooth and rough surfaces at large displacement. TULLIS and WEEKS (1986) argued that the similarity in steady-state a-b values was an indication of wear and gouge accumulation in the bare surface experiments, and that after a running-in period, similar mechanisms operated within the simulated and naturally-produced gouge. Subsequent results, however, showed that a-b for gouge and bare surfaces diverge at larger displacements (BEELER *et al.*, 1993).

An important difference between the bare surface and gouge cases is that thick gouge may remain poorly consolidated, whereas thin layers of very fine gouge (such as produced by wear between smooth surfaces) may become indurated, with shear localizing in narrow zones (e.g., MARONE *et al.*, 1992; GU and WONG, 1994).

MARONE *et al.* (1990) showed that thick, unconsolidated gouge exhibits velocity strengthening due to dilation. Recent work on a grain-bridge model supports this view, showing that rough surfaces and small displacements favor velocity strengthening (SAMMIS and STEACY, 1994).

Our data are consistent with this interpretation. The similarity in a-b values for rough and smooth surfaces after slip of 50–60 mm is consistent with narrowing of the difference in friction level for the two roughnesses (Figures 5 and 7). Furthermore, velocity strengthening and the gradual onset of yielding for rough surfaces at low displacement is similar to observations for gouge deformation (MARONE *et al.*, 1990). The transition we observe to velocity weakening for rough surfaces is consistent with lesser dilation for localized shear (BEELER *et al.*, 1993; MARONE, 1993).

Micromechanics of Rate and State Effects

Enhanced asperity interlocking between rough surfaces compared with smooth surfaces would imply higher wear rates and greater gouge accumulation for rough surfaces (e.g., WANG and SCHOLZ, 1994). This may explain our observation that D_c increases slightly with displacement for rough surfaces since D_c scales with gouge layer thickness for a given shear strain (MARONE and KILGORE, 1993).

Another important feature of our data is the second state variable observed for rough surfaces. Others have observed two characteristic distances for smoother surfaces (e.g., RUINA, 1983; TULLIS and WEEKS, 1986; COX, 1990) and suggested that they correspond to two distinct features of the roughness spectrum (J. DIETERICH, pers. comm.) or to some combination of roughness and microstructural features of the gouge (COX, 1990). Although we cannot rule out the former possibility, the roughness data and asperity characteristics do not indicate two distinct maxima or other bimodal characteristics.

COX (1990) suggested that the longer characteristic displacement, D_{c2}, was produced by structure in the gouge and the shorter one was due to surface properties. Our data from rough surfaces suggest that D_{c2} is a surface effect, since it disappears with slip, and that the shorter characteristic displacement, D_{c1}, is a property of the gouge since it gradually evolves to a steady-state value. Thus, there may be a dramatic difference in the bare surface constitutive behavior of rough and smooth surfaces, but this is hidden because the two D_c's are very similar for the smoother surfaces.

This interpretation is consistent with the observed increase in D_{c1} values with accumulated slip and a model in which D_c for a gouge zone is produced by superposition of the d_c's from individual particle-particle contacts within the gouge layer (MARONE and KILGORE, 1993). MARONE and KILGORE (1993) showed that D_c scales with shear strain and shear zone thicknesses within a gouge layer and thus the observed increase in D_{c1} for rough surfaces is consistent with accumulation of

gouge via wear. Systematic measurements of gouge thicknesses were not carried out, but gouge was observed on the surfaces (thickness = 100 μm) in post-experiment examination.

Our data indicate that a-b and D_c both evolve in response to wear and gouge formation, but that D_c attains a value which depends on the initial roughness, whereas the steady-state a-b value is independent of the initial roughness. Whether this result extends to greater net displacement remains to be tested, but the results of experiments on gouge sheared within smaller and smoother surfaces (BEELER *et al.*, 1993) indicate further changes in a-b at larger net displacements than reached in our experiments.

Nevertheless, the observation that a-b is approximately roughness-independent for large slip, whereas D_c increases with slip for rough surfaces, implies that a-b and D_c respond to an overlapping but not identical set of micromechanical features and processes. This is consistent with the idea that D_c represents a composite transient effect for many slip surfaces (e.g., interparticle contacts within the actively shearing region) each with the same a-b. In that case, D_c would scale with gouge thickness, whereas a-b would not, which is consistent with rougher surfaces producing more gouge and hence a thicker region of localized shear than smooth surfaces.

If natural faults exhibit similar characteristics, our data may help explain why some faults seem to become more aseismic with accumulated offset (WESNOUSKY, 1990), as implied by our observation of increasing D_c with increased net offset and gouge thickness.

Conclusions

We studied the frictional behavior and constitutive parameters of rough and smooth bare-rock surfaces. Our data show that rough surfaces exhibit velocity strengthening frictional behavior for small net displacements and that the friction velocity dependence and characteristic friction distance evolve with displacement. After 40–50 mm of slip, the friction velocity dependence for rough surfaces became velocity weakening of similar magnitude to that observed for smooth surfaces. The friction velocity dependence and characteristic friction distance for smooth surfaces did not evolve with displacement. For rough surfaces the characteristic friction distance increased with accumulated displacement, in agreement with models in which D_c is controlled by the width of shear within fault gouge. Although the rms and peak-to-trough roughness of our rough and smooth surfaces differed substantially, the characteristic friction distance D_{c1} was the same for both surfaces. Rough surfaces exhibited a second state variable and characteristic friction distance D_{c2} of about 20 μm for shear displacements less than 30 mm. We interpret the longer characteristic distance as a surface effect and the shorter distance as a property of the gouge.

Acknowledgements

We would like to acknowledge the encouragement and financial support of B. Hobbs and the CSIRO Division of Geomechanics. We also benefitted from the critical reviews of N. Beeler, M. Blanpied, J. Weeks, and an anonymous reviewer. CM gratefully acknowledges helpful discussions with B. Romanowicz and N. Yoshioka, and financial support from the Berkeley Seismographic Station, NSF grant EAR 91–18249, and IGPP grant 92–49. SC was partially supported by USGS grant 14–08–0001–G1191. We also thank Peter Muir of Layton Granite Pty., Sunshine, Vic., who supplied precision-sized rock samples and technical assistance with sandblasting.

REFERENCES

ARCHARD, J. F. (1957), *Elastic Deformation and the Laws of Friction*, Proc. R. Soc. London, Ser. A *243*, 190–205.

AKI, K. (1957), *Magnitude-frequency Relation for Small Earthquakes: A Clue to the Origin of f_{max} of Large Earthquakes*, J. Geophys. Res. *92*, 1349–1355.

BIEGEL, R. L., SAMMIS, C. G., and DIETERICH, J. H. (1989), *The Frictional Properties of a Simulated Gouge Having a Fractal Particle Distribution*, J. Struct Geology *11*, 827–846.

BEELER, N. M., TULLIS, T. E., and WEEKS, J. D. (1993), *The Contribution of Simulated Gouge to the Velocity Dependence of Experimental Granite Faults*, EOS, Trans. Amer. Geophys. Un. *74*, 296.

BLANPIED, M. L., and TULLIS, T. E. (1986), *The Stability and Behavior of a Frictional System with a Two State Variable Constitutive Law*, Pure and Appl. Geophys. *124*, 415–430.

BLANPIED, M. L., LOCKNER, D. A., and BYERLEE, J. D. (1991), *Fault Stability Inferred from Granite Sliding Experiments at Hydrothermal Conditions*, Geophys. Res. Lett. *18*, 609–612.

CHESTER, F. M. (1994), *Effects of Temperature on Friction: Constitutive Equations and Experiments with Quartz Gouge*, J. Geophys. Res. *99*, 7247–7261.

COX, S. J. D., *Velocity dependent friction in a large direct shear experiment on gabbro.* In *Deformation Mechanisms, Rheology, and Tectonics* (eds. Knipe, R. J, and Rutter, E.H.) (Geol. Soc. London 1990) Spec. Pub. *54*, pp. 63–70.

DIETERICH, J. H. (1979), *Modeling of Rock Friction: 1. Experimental Results and Constitutive Equations*, J. Geophys. Res. *84*, 2161–2168.

DIETERICH, J. H., *Constitutive properties of faults with simulated gouge.* In *Mechanical Behavior of Crustal Rocks* (eds. Carter, N. L., Friedman, M., Logan, J. M., and Stearns, D. M.) (AGU Monograph *24*, 1981) pp. 103–120.

DIETERICH, J. H., *A model for the nucleation of earthquake slip.* In *Earthquake Source Mechanics* (eds. Das, S., BOATWRIGHT, J., and SCHOLZ, C H.) (AGU Monograph *37*, 1986) pp. 37–47.

GU, Y., and WONG, T.-f. (1994), *Development of Shear Localization in Simulated Quartz Gouge: Effect of Cumulative Slip and Gouge Particle Size*, Pure and Appl. Geophys. *143*, 387–423.

IDA, Y. (1973), *The Maximum Ground Acceleration of Seismic Ground Motion.* Bull. Seismol. Soc. Am. *63*, 959–968.

KUWAHARA, Y., OHNAKA, M., YAMAMOTO, K., and HIRASAWA, T. (1988), *Accelerating Process of Rupture Propagation during Stick-slip Failure Instability*, Seis. Res. Lett. *59*, 2.

LI, V. C., *Mechanics of shear rupture applied to earthquake zones.* In *Fracture Mechanics of Rock* (ed. Atkinson, B.) (Academic Press, London, 1987) pp. 351–428.

LOCKNER, D. A., SUMMERS, R., and BYERLEE, J. D. (1986), *Effects of Temperature and Sliding Rate on Frictional Strength of Granite*, Pure and Appl. Geophys. *124*, 445–469.

MARONE, C. (1993), *Micromechanics of Rate- and State-dependent Friction in Simulated Fault Gouge*, EOS, Trans. Amer. Geophys. Un. *74*, 296.

MARONE, C., and SCHOLZ, C. H. (1988), *The Depth of Seismic Faulting and the Upper Transition from Stable to Unstable Slip Regimes*, Geophys. Res. Lett. *15*, 621–624.

MARONE, C., and KILGORE, B. (1993), *Scaling of the Critical Slip Distance for Seismic Faulting with Shear Strain in Fault Zones*, Nature *362*, 618–621.

MARONE, C., RALEIGH, C. B., and SCHOLZ, C. H. (1990), *Frictional Behavior and Constitutive Modeling of Simulated Fault Gouge.*, J. Geophys. Res. *95*, 7007–7025.

MARONE, C., HOBBS, B. E., and ORD, A. (1992), *Coulomb Constitutive Laws for Friction: Contrasts in Frictional Behavior for Distributed and Localized Shear*, Pure and Appl. Geophys. *139*, 195–214.

OHNAKA, M., and YAMASHITA, T. (1989), *A Cohesive Zone Model for Dynamic Shear Faulting Based on Experimentally Inferred Constitutive Relation and Strong Motion Source Parameters*, J. Geophys. Res. *94*, 4089–4104.

OHNAKA, M., and KUWAHARA, Y. (1990), *Characteristic Features of Local Breakdown near a Crack-tip in the Transition Zone from Nucleation to Dynamic Rupture during Stick-slip Shear Failure*, Tectonophys. *175*, 197–220.

OKUBO, P. G. (1989), *Dynamic Rupture Modeling with Laboratory-derived Constitutive Relations*, J. Geophys. Res. *94*, 12,321–12,335.

OKUBU, P. G., and DIETERICH, J. H. (1984), *Effects of Physical Fault Properties on Frictional Instabilities Produced on Simulated Faults*, J. Geophys. Res. *89*, 5817–5827.

PISARENKO, D., and MORA, P. (1994), *Velocity Weakening in a Dynamical Model of Friction*, Pure and Appl. Geophys. *143*, 61–87.

POWER, W. L., and TULLIS, T. E. (1992), *The Contact between Opposing Fault Surfaces at Dixie Valley, Nevada, and Implications for Fault Mechanics*, J. Geophys. Res. *97*, 14,425–14,435.

PRESS, W. H., FLANNERY, B. P., TEUKOLSHY, S. A., and VETTERLING, W. T., *Numerical Recipes in C* (Cambridge, 1988) 475 pp.

RABINOWICZ, E. (1951), *The Nature of the Static and Kinetic Coefficients of Friction*, J. Appl. Phys. *22*, 1373–1379.

REINEN, L. A., and WEEKS, J. D. (1993), *Determination of Rock Friction Constitutive Parameters using an Iterative Least-squares Inversion Method.* J. Geophys. Res. *98*, 15,937–15,950.

REINEN, L. A., WEEKS, J. D., and TULLIS, T. E. (1991), *The Frictional Behavior of Serpentinite: Implications for Aseismic Creep on Shallow Crustal Faults*, Geophys. Res. Lett. *18*, 1921–1924.

REINEN, L. A., WEEKS, J. D., and TULLIS, T. E. (1994), *The Frictional Behavior of Lizardite and Antigorite Serpentinites: Experiments, Constitutive Models, and Implications for Natural Faults*, Pure and Appl. Geophys. *143*, 317–358.

RICE, J. R. (1993), *Spatio-temporal Complexity of Slip on a Fault*, J. Geophys. Res. *98*, 9885–9907.

RICE, J. R., and RUNIA, A. L. (1983), *Stability of Steady Frictional Slipping*, J. Appl. Mech. *50*, 343–349.

RICE, J. R., and TSE, S. T. (1986), *Dynamic Motion of a Single Degree of Freedom System Following a Rate and State-dependent Friction Law.*, J. Geophys. Res. *91*, 521–530.

RUINA, A. (1983), *Slip Instability and State Variable Friction Laws*, J. Geophys. Res. *88*, 10359–10370.

SAMMIS, C. G., and STEACY, S. (1994), *The Micromechanics of Friction in a Granular Layer*, Pure and Appl. Geophys. *142*, 777–794.

SCHOLZ, C. H. (1988), *The Critical Slip Distance for Seismic Faulting*, Nature *336*, 761–763.

SCHOLZ, C. H., *The Mechanics of Earthquakes and Faulting* (Cambridge University Press, 1990) 439 pp.

TSE, S. T., and RICE, J. R. (1986), *Crustal Earthquake Instability in Relation to the Depth Variation of Frictional Slip Properties*, J. Geophys. Res. *91*, 9452–9472.

TULLIS, T. E. (1988), *Rock Friction Constitutive Behavior from Laboratory Experiments and its Implications for an Earthquake Prediction Field Monitoring Program*, Pure and Appl. Geophys. *126*, 555–588.

TULLIS, T. E., and WEEKS, J. D. (1986), *Constitutive Behavior and Stability of Frictional Sliding of Granite*, Pure and Appl. Geophys. *124*, 383–414.

WANG, W., and SCHOLZ, C. H. (1994), *Micromechanics of the Velocity and Normal Stress Dependence of Rock Friction*, Pure and Appl. Geophys. *143*, 303–315.

WESNOUSKY, S. G. (1990), *Seismicity as a Function of Cumulative Geologic Offset: Some Observations from Southern California*, Bull. Seismol. Soc. Am. *80*, 1374–1381.

WONG, T.-f., GU, Y., YANAGIDANI, T., and ZHAO, Y., *Stabilization of faulting by cumulative slip*. In *Fault Mechanics and Transport Properties of Rock* (eds. Evans, B., and Wong, T.-f.) (Academic Press Ltd., 1992) pp. 119–143.

YAMADA, K., TAKEDA, N., KAGAMI, J., and NAOI, T. (1978), *Surface Density of Asperities and Real Distribution of Asperity Heights on Rubbed Surfaces*, Wear *47*, 5–20.

YOSHIOKA, N., and SCHOLZ, C. H. (1989), *Elastic Properties of Contacting Surfaces under Normal and Shear Loads 1. Theory.*, J. Geophys. Res. *94*, 17,681–17,690.

(Received September 21, 1993, revised May 25, 1994, accepted May 27, 1994)